Capacitively-Loaded Thin-Film Lithium Niobate Modulator With Ultra-Flat Frequency Response

Xuecheng Liu, Bing Xiong, *Member, IEEE*, Changzheng Sun, *Member, IEEE*, Zhibiao Hao, Lai Wang, Jian Wang, *Member, IEEE*, Yanjun Han, Hongtao Li, and Yi Luo

***Abstract*— Traveling-wave electro-optic (E-O) modulators based on thin-film lithium niobate (TFLN) have attracted much attention recently, as low half-wave voltage (V_π) and wide modulation bandwidth can be realized with a small footprint. A flat E-O response of the modulator relies on low microwave loss, perfect velocity match and suitable terminal resistance. In this Letter, we present velocity-matched TFLN modulator based on low-loss capacitively-loaded traveling-wave electrodes (CL-TWEs) with an on-chip terminal resistor. The effect of termination resistance on the E-O frequency response is theoretically analyzed and experimentally confirmed. The TFLN modulator with 6-mm modulation length exhibit a V_π of 2.7 V and a 6.4-dB electrical bandwidth over 160 GHz. By adopting a termination resistance slightly lower than the characteristic impedance of the CL-TWEs, an ultra-flat E-O response has been demonstrated with fluctuation less than 1-dB up to 50 GHz, consistent with the theoretical prediction.**

***Index Terms*— Thin-film lithium niobate, electrooptic modulators, capacitively-loaded electrodes, frequency response.**

I. Introduction

As a fundamental part of broadband microwave photonic links, electro-optic (E-O) modulators have attracted sustained attention for decades. E-O modulators based on III-V compound semiconductors or silicon exhibit high modulation efficiency, but suffer from large optical loss and microwave absorption [1], [2]. On the other hand, lithium niobate ($LiNbO_3$) shows special potential for high-performance modulators due to its large E-O coefficient (30.8 pm/V) and wide transparency window (350-5000 nm). However, conventional $LiNbO_3$ modulators with weakly-confined waveguides are too bulky for integration [3].

Thin-film lithium niobate (TFLN) prepared by crystal ion slicing and directly bonding allows for optical waveguides with strong confinement [4], leading to reduced device footprint and improved electric field loading efficiency of the modulator. TFLN modulators have demonstrated low half-wave voltage (V_π) as well as large modulation bandwidth at millimeter-scale modulation length [5]–[7]. In particular, we proposed to employ periodic capacitively-loaded traveling-wave electrodes (CL-TWEs) in TFLN modulators [8], and it was subsequently demonstrated to further break the bandwidth-voltage limitation [9]–[12].

For applications such as microwave photonic radars [13], especially when a clean spatial beam and a sharp temporal impulse response are required for the multielement beamformer with phase-coded RF pulse [14], both an ultra-flat frequency response and a low V_π are required for optical modulators. However, the conductor loss ($\propto \sqrt{f}$) of the traveling-wave electrodes leads to a steep roll-off in the E-O response at low frequencies, which is aggravated by fluctuations of characteristic impedance and microwave velocity. It has been verified in previous studies [15]–[17] that a lower terminal resistance brings about an initial rise in the E-O response, thus can be employed to compensate the drop-off at low frequencies for band equalization, but at the cost of reduced static modulation depth and increased microwave reflection. In this work, we demonstrate 160 GHz electrical bandwidth for TFLN modulator with optimized CL-TWEs and on-chip NiCr resistor [18]. The 6-mm-long modulator exhibits a low half-wave voltage of 2.7 V, and the impact of different terminators on the E-O response are theoretical analyzed and experimentally demonstrated. By adopting a suitable terminal resistance slightly lower than the characteristic impedance of the CL-TWEs, ultra-flat E-O response with less than 1-dB fluctuation is secured up to 50 GHz, which is of great significance for high-performance microwave photonic links.

II. Device Design

The schematic structure of our TFLN modulator is shown in Fig. 1(a). Modulation arms connected by Y-branches are formed on X-cut TFLN to realize parallel push-pull Mach–Zehnder (MZ) configuration. The CL-TWEs are terminated by an on-chip NiCr resistor [18]. A 90-degree bent feedline is used to connect the CL-TWEs to microwave probes. The cross-sectional view of the modulation region is shown in Fig. 1(b). $LiNbO_3$-SiO_2 hybrid waveguide is adopted to ensure low optical absorption for a reduced electrode gap [10], which contains a 300-nm-deep ridge waveguide etched on 600-nm-thick TFLN and covered by a 100-nm-thick silica layer. The gap between the T-rails on both sides of the optical waveguide

Manuscript received 15 February 2022; revised 19 May 2022; accepted 23 May 2022. Date of publication 26 May 2022; date of current version 3 August 2022. This work was supported in part by the National Key Research and Development Program of China under Grant 2018YFB2201701; in part by the National Natural Science Foundation of China under Grant 61975093, Grant 61927811, Grant 61991443, Grant 61822404, Grant 61974080, Grant 61904093, and Grant 61875104; in part by the Key Laboratory Program of the Beijing National Research Centre for Information Science and Technology (BNRist) under Grant BNR2019ZS01005; in part by the China Postdoctoral Science Foundation under Grant 2019T120090; and in part by the Collaborative Innovation Centre of Solid-State Lighting and Energy-Saving Electronics. *(Corresponding author: Bing Xiong.)*

The authors are with the Beijing National Research Centre for Information Science and Technology (BNRist), Department of Electronic Engineering, Tsinghua University, Beijing 100084, China (e-mail: bxiong@mail.tsinghua.edu.cn).

Color versions of one or more figures in this letter are available at https://doi.org/10.1109/LPT.2022.3178214.

Digital Object Identifier 10.1109/LPT.2022.3178214

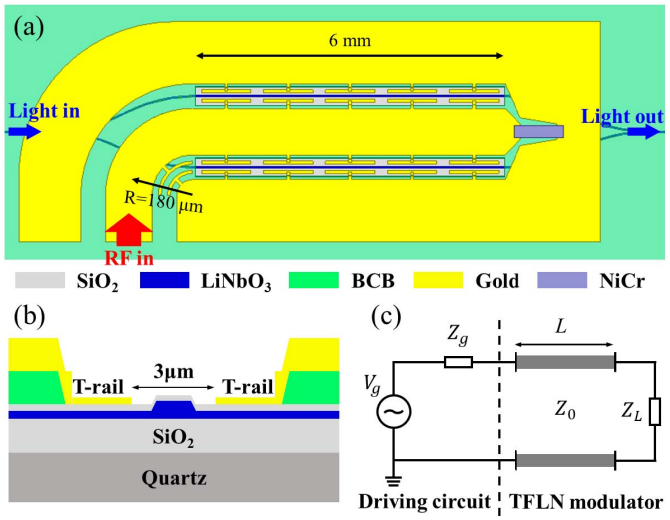

Fig. 1. (a) Schematic of our TFLN modulator. (b) Cross-sectional diagram of the modulation arm. (c) Equivalent circuit for the TFLN modulator with on-chip terminal.

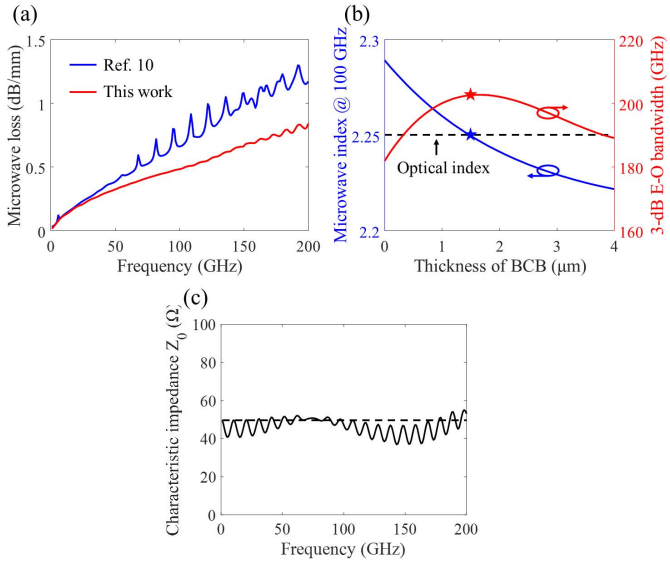

Fig. 2. (a) Simulated microwave loss compared with our previous work. (b) Variation of the microwave index and the 3-dB E-O bandwidth with the BCB layer thickness. (c) Simulated characteristic impedance Z_0 of the CL-TWEs.

is set as 3 μm for enhanced electric field loading efficiency. Compared with our previous work [10], the unloaded electrodes have been optimized for reduced microwave loss, and a benzocyclobutene (BCB) layer is formed beneath the unloaded electrodes for perfect velocity matching. The equivalent circuit of the traveling-wave modulator can be modeled as Fig. 1(c). V_g is the amplitude of the driving signal, and the source impedance Z_g is taken to be 50 Ω. The CL-TWEs can be modeled as a transmission line with characteristic impedance Z_0, which is terminated by a load resistance Z_L.

Based on the transmission line model shown in Fig. 1(c), the average voltage applied on the modulator can be expressed as [15]:

$$V_{avg}(\omega_m) = \frac{1}{L}\int_0^L \frac{V_g(1+\rho_1)e^{i\beta_0 L}(e^{i(\beta_e-\beta_0)x}+\rho_2 e^{-i(\beta_e+\beta_0)x})}{2(e^{i\beta_e L}+\rho_1\rho_2 e^{-i\beta_e L})}dx \quad (1)$$

$$\rho_1 = \frac{Z_0 - Z_g}{Z_0 + Z_g} \quad (2)$$

$$\rho_2 = \frac{Z_L - Z_0}{Z_L + Z_0} \quad (3)$$

where L is the length of the modulation region, $\beta_e - \beta_o$and $\beta_e + \beta_o$ represent the wave vector walk-off between the optical and the transmitted/reflected microwave signals, respectively, while ρ_1 and ρ_2 denote the input/output reflection coefficients of the microwave transmission line. The small signal frequency response can be defined as:

$$M(f) = 20\log_{10}\left[\frac{V_{avg}(2\pi f)}{V_{avg}(2\pi f_0)}\right] \quad (4)$$

where the reference frequency f_0 is usually taken to be dc or a low frequency on the order of MHz.

Then microwave characteristics of CL-TWEs are obtained by a full-wave simulation based on finite element method (FEM). To achieve a flat E-O response, the dimensions of the unloaded electrodes are adjusted to reduce the microwave transmission loss. The thickness of the gold electrode is set as 4 μm, while the signal electrode width and the gap between unloaded electrodes are taken to be 80 μm and 20 μm, respectively. This results in a 30% reduction of simulated microwave loss compared with our previous work [10]. The inner slot of the 90-degree bent feedlines are designed as slow-wave structure to equalize the electrical length with outer slot, so as to suppress the microwave resonances at high frequencies [19], as shown in Fig. 2(a). Moreover, to achieve perfect velocity matching between the microwave signal and the optical mode, the thickness of the BCB layer beneath the main electrodes is adjusted to fine-tune the microwave index. As the BCB layer thickness increases, more electric field resides in the low dielectric constant region, which results in a gradual reduction of the microwave index, as confirmed by the simulation results shown in Fig. 2(b). As the major part of the modulation electric field is distributed between T-rails, this allows an accurately adjustment of the microwave index without degrading the modulation efficiency. Also plotted in Fig. 2(b) is the variation of the 3-dB E-O bandwidth with the BCB layer thickness, assuming a standard 50-Ω terminal resistance. A 1.5-μm-thick BCB layer is found to improve the 3-dB bandwidth by more than 20 GHz. The simulated characteristic impedance Z_0 of the CL-TWEs is shown in Fig. 2(c), which varies around 50 Ω.

In a traveling-wave modulator, both the characteristic impedance of the transmission line and the terminal load are usually taken to be 50 Ω to minimize microwave reflection. However, the terminal resistance can be tuned to adjust the E-O response of the modulator. The effect of different terminal resistance on modulator E-O response can be calculated from equations (1) and (4) with the simulated microwave transmission characteristics. The average voltages on the modulator under different terminals are plotted in Fig. 3(a), assuming a V_g of 1 V. The E-O responses in Fig. 3(b) reveal that a terminal resistance Z_L lower than the characteristic impedance Z_0

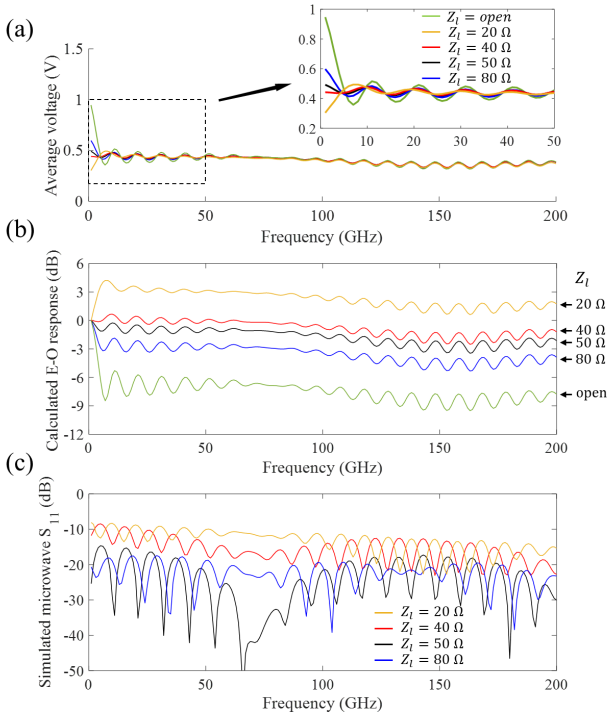

Fig. 3. Calculated (a) average voltages (b) E-O responses and (c) microwave reflection S_{11} under different terminal resistance.

of CL-TWEs results in enhanced E-O response, which can be explained by the negative reflection coefficient ρ_2, i.e. Z_L less than Z_0, results in an initial rise in the E-O response, whereas for Z_L greater than Z_0, the E-O responses exhibits a sharp drop-off at low frequencies. The roll off of the E-O response at high frequencies is more or less similar for different terminal resistances. Meanwhile, the electrical reflections shown in Fig. 3(c) remains below -10 dB for Z_L not too far deviated from Z_0. In other words, a suitable terminal resistance Z_L slightly lower than the characteristic impedance Z_0 of the CL-TWEs can be adopted to compensate for the drop-off at low frequencies to obtain an ultra-flat E-O response.

III. Device Fabrication and Characterization

The proposed modulators are fabricated on a 600-nm-thick X-cut TFLN provided by NanoLN. The TFLN film is formed on 500-μm-thick quartz substrate with 2-μm-thick silica as the bonding layer. The optical waveguide patterns are defined by electron beam lithography (EBL) with hydrogensilsesquioxane (HSQ) resist, and transferred to the TFLN by argon-based reactive ion etching (RIE) to form 1-μm-wide and 300-nm-thick ridge waveguides. The waveguides are then encapsulated with 100-nm-thick silica layer by plasma enhanced chemical vapor deposition (PECVD). The wafer is cladded with a 1.5-μm-thick photosensitive BCB layer by spin-coating. The BCB layer around the modulation arms is selectively removed by developer, whereas the remaining part is utilized for microwave index control and isolation between optical Y-branches and metal electrodes. A two-step fabrication process is employed for the CL-TWEs: First a lift-off process with polymethylmethacrylate (PMMA) exposed by EBL is employed to form T-rails with high positional accuracy.

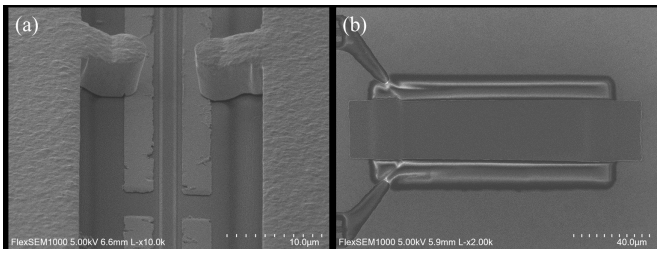

Fig. 4. SEM images of (a) the modulation region containing narrow-gap T-rails and (b) the on-chip NiCr terminal resistor.

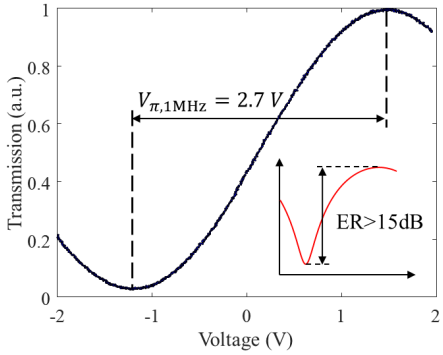

Fig. 5. Normalized optical transmission as a function of driving voltage.

Next, the main electrodes are defined by contact UV lithography, and thickened to more than 4 μm by electroplating to reduce the microwave loss. The CL-TWEs are terminated with an on-chip NiCr resistor formed by a lift-off process. The scanning electron microscope (SEM) images of the modulation region and the on-chip terminal are shown in Fig. 4.

The modulator is characterized by end-butt coupling via two tapered fibers. As the photorefractive effect of $LiNbO_3$ may result in measurement errors of V_π with DC scanning, 1 MHz triangular-wave voltage signal is fed to the modulator through a G-S-G probe. The optical extinction curve is obtained on a modulator with open terminal to avoid inconsistent voltage division on the modulator caused by different terminal resistance Z_L. As shown in Fig. 5, a low V_π of 2.7 V is obtained for 6 mm modulation length, corresponding to a half-wave voltage length product $V_\pi L$ of 1.62 V·cm, consistent with our previous results [10]. The fiber-to-fiber loss is measured as 16 dB, which consists of 4 dB on-chip loss and 6 dB/facet coupling loss due to the mode field mismatch between the lensed fiber and the optical waveguide.

The high-frequency modulation behavior of the modulators are then characterized. The microwave transmission properties of the CL-TWEs are tested first on the modulator with open terminal. High-frequency microwave signal from a Keysight N5290A vector network analyzer (VNA) equipped with a frequency extension module up to 170 GHz is fed to the CL-TWEs via two microwave probes. The measured S-parameters are shown in Fig. 6(a). The 6.4-dB electrical bandwidth is measured to be 160 GHz, indicating the low-loss transmission property of the CL-TWEs. Compared with our previous results [10], the electrical resonances are suppressed, thanks to the optimized 90-degree bent feedlines. The measured microwave loss is higher than the simulation results, which may be attributed to the high resistance of the

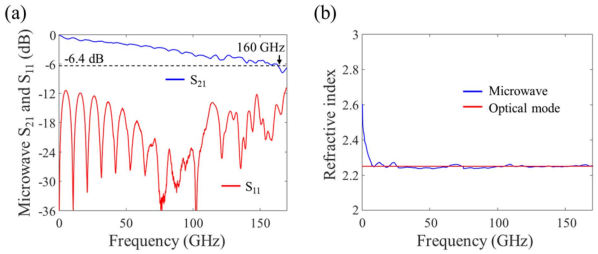

Fig. 6. (a) Measured microwave transmission S_{21} and reflection S_{11} of the CL-TWEs. (b) The extracted microwave index.

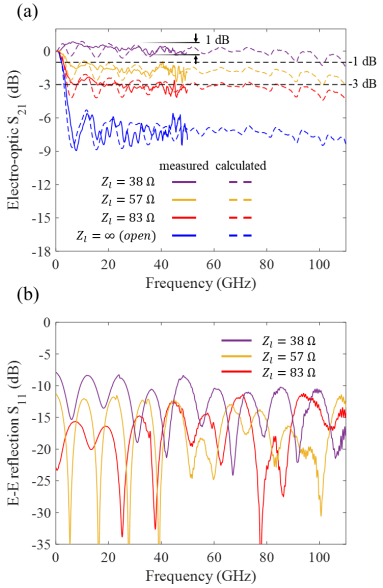

Fig. 7. (a) The measured E-O responses with different terminal resistances. (b) The microwave reflection S_{11} with different on-chip resistors.

fabricated T-rails. The extracted microwave index shown in Fig. 6(b) reveals a perfect match with the optical group index (n_g ~2.25), indicating that the E-O frequency response is only affected by microwave loss and impedance matching condition in this case.

For E-O response characterization, the modulated signal is fed back to the VNA via a high-speed photodetector (u^2t XPDV2120R) with a bandwidth up to 50 GHz. The calibrated E-O responses for modulators with different terminal resistances are plotted in Fig. 7(a). The extended E-O responses are calculated by the transmission line model with measured microwave parameters, and are consistent with the measurement results over the test frequency band. For the TFLN modulator with 38 Ω on-chip terminal resistance, the E-O response reveals an initial rise and exhibits an ultra-flat frequency response with fluctuations less than 1 dB up to 50 GHz. Meanwhile, the electrical reflection S_{11} shown in Fig. 7(b) remains approximately below −10 dB, thus avoiding the negative influence on the E-O modulation and electrical driver.

IV. Conclusion

TFLN modulator with ultra-flat E-O response is implemented with low-loss CL-TWEs terminated by on-chip resistor. 2.7 V V_π and 160 GHz electrical bandwidth are realized simultaneously with 6-mm modulation length. The dependence of E-O response on terminal resistance is theoretically analyzed and experimentally confirmed. Ultra-flat E-O response with less than 1-dB fluctuation up to 50 GHz is obtained by adopting a terminal resistance slightly lower than the characteristic impedance of the CL-TWEs, in consistence with our simulations. This demonstration provides a design method for improved frequency response of TFLN modulators.

References

[1] Y. Ogiso *et al.*, "80-GHz bandwidth and 1.5-V V_π InP-based IQ modulator," *J. Lightw. Technol.*, vol. 38, no. 2, pp. 249–255, Jan. 15, 2020, doi: 10.1109/JLT.2019.2924671.

[2] G. T. Reed, G. Mashanovich, F. Y. Gardes, and D. J. Thomson, "Silicon optical modulators," *Nature Photon.*, vol. 4, pp. 518–526, Jul. 2010, doi: 10.1038/nphoton.2010.179.

[3] E. L. Wooten *et al.*, "A review of lithium niobate modulators for fiber-optic communications systems," *IEEE J. Sel. Topics Quantum Electron.*, vol. 6, no. 1, pp. 69–82, Jan. 2000, doi: 10.1109/2944.826874.

[4] G. Poberaj, H. Hu, W. Sohler, and P. Günter, "Lithium niobate on insulator (LNOI) for micro-photonic devices," *Laser Photon. Rev.*, vol. 6, no. 4, pp. 488–503, 2012, doi: 10.1002/lpor.201100035.

[5] C. Wang *et al.*, "Integrated lithium niobate electro-optic modulators operating at CMOS-compatible voltages," *Nature*, vol. 562, pp. 101–104, Sep. 2018, doi: 10.1038/s41586-018-0551-y.

[6] M. He *et al.*, "High-performance hybrid silicon and lithium niobate Mach–Zehnder modulators for 100 Gbit s^{-1} and beyond," *Nature Photon.*, vol. 13, no. 5, pp. 359–364, May 2019, doi: 10.1038/s41566-019-0378-6.

[7] A. N. R. Ahmed, S. Shi, A. Mercante, S. Nelan, P. Yao, and D. W. Prather, "High-efficiency lithium niobate modulator for k band operation," *APL Photon.*, vol. 5, no. 9, Sep. 2020, Art. no. 091302, doi: 10.1063/5.0020040.

[8] X. Liu *et al.*, "Low half-wave-voltage thin film $LiNbO_3$ electro-optic modulator based on a compact electrode structure," in *Proc. Asia Commun. Photon. Conf./Int. Conf. Inf. Photon. Opt. Commun. (ACP/IPOC)*, 2020, p. M4A.144, doi: 10.1364/ACPC.2020.M4A.144.

[9] P. Kharel, C. Reimer, K. Luke, L. He, and M. Zhang, "Breaking voltage–bandwidth limits in integrated lithium niobate modulators using micro-structured electrodes," *Optica*, vol. 8, no. 3, p. 357, Mar. 2021, doi: 10.1364/OPTICA.416155.

[10] X. Liu *et al.*, "Wideband thin-film lithium niobate modulator with low half-wave-voltage length product," *Chin. Opt. Lett.*, vol. 19, no. 6, 2021, Art. no. 060016, doi: 10.3788/COL202119.060016.

[11] G. Chen *et al.*, "High performance thin-film lithium niobate modulator on a silicon substrate using periodic capacitively loaded traveling-wave electrode," *APL Photon.*, vol. 7, no. 2, Feb. 2022, Art. no. 026103, doi: 10.1063/5.0077232.

[12] M. Xu *et al.*, "Dual-polarization thin-film lithium niobate in-phase quadrature modulators for terabit-per-second transmission," *Optica*, vol. 9, no. 1, p. 61, Jan. 2022, doi: 10.1364/OPTICA.449691.

[13] S. Pan and Y. Zhang, "Microwave photonic radars," *J. Lightw. Technol.*, vol. 38, no. 19, pp. 5450–5484, Oct. 1, 2020, doi: 10.1109/JLT.2020.2993166.

[14] O. Raz, S. Barzilay, R. Rotman, and M. Tur, "Submicrosecond scan-angle switching photonic beamformer with flat RF response in the C and X bands," *J. Lightw. Technol.*, vol. 26, no. 15, pp. 2774–2781, Aug. 1, 2008, doi: 10.1109/JLT.2008.927150.

[15] S. H. Lin and S.-Y. Wang, "High-throughput GaAs PIN electrooptic modulator with a 3-dB bandwidth of 9.6 GHz at 1.3 μm," *Appl. Opt.*, vol. 26, no. 9, pp. 1696–1700, May 1987, doi: 10.1364/AO.26.001696.

[16] H. Yu and W. Bogaerts, "An equivalent circuit model of the traveling wave electrode for carrier-depletion-based silicon optical modulators," *J. Lightw. Technol.*, vol. 30, no. 11, pp. 1602–1609, Jun. 1, 2012, doi: 10.1109/JLT.2012.2188779.

[17] H. Xu *et al.*, "High-speed silicon modulator with band equalization," *Opt. Lett.*, vol. 39, no. 16, p. 4839, Aug. 2014, doi: 10.1364/OL.39.004839.

[18] X. Liu *et al.*, "Broadband capacitive-loaded thin-film lithium niobate modulator with on-chip terminal resistor," in *Proc. Asia Commun. Photon. Conf.*, 2021, p. T1I.5, doi: 10.1364/ACPC.2021.T1I.5.

[19] X. Liu *et al.*, "A highly compact thin-film lithium niobate modulator with low half-wave voltage," in *Proc. Opt. Fiber Commun. Conf. (OFC)*, 2022, p. Th1J.6, doi: 10.1364/OFC.2022.Th1J.6.